

1
2
3

4 **Statistical properties of flux closure induced by solar**
5 **wind dynamic pressure fronts.**

6
7

8 B. Hubert⁽¹⁾, C. Blockx⁽¹⁾, S.E. Milan⁽²⁾, S.W.H. Cowley⁽²⁾

9

- 10 1. Laboratory for Planetary and Atmospheric Physics, University of Liège, Belgium
11 2. Department of Physics & Astronomy, University of Leicester, Leicester LE1 7RH, UK

12
13
14

J. Geophys. Res., 114, A07211, doi:10.1029/2008JA013813.

15 Abstract

16 We present a statistical study of flux closure intervals induced by solar wind dynamic
17 pressure fronts. We consider that a dynamic pressure front reaches the Earth when a dayside
18 subauroral proton flash is observed in the SI2 channel of the IMAGE-FUV experiment. This
19 pragmatic criterion selects both weak and strong pressure fronts. It is found that the
20 preconditioning of the magnetosphere prior to the pressure pulse arrival mainly governs the
21 magnetospheric response to a weak solar wind dynamic pressure front. This preconditioning
22 includes the amount of open magnetic flux available in the magnetosphere prior to the
23 pressure front arrival and the size of the magnetospheric cavity. However, in the case of a
24 strong pressure pulse, the magnetospheric response is more sensitive to the solar wind
25 properties characterizing the dynamic pressure front. Not only is the pressure jump important,
26 but also the variation of the solar wind velocity and IMF magnitude. In overall terms, we find
27 that a strong dynamic pressure front is typically characterized by a dynamic pressure increase
28 larger than ~ 2.8 nPa that takes place on time scales of the order of a few minutes.

29 1. Introduction

30 The solar wind is the plasma outflow from the solar atmosphere. It carries the
31 interplanetary magnetic field (IMF), which is frozen in the solar plasma. When the solar wind
32 reaches the Earth, the geomagnetic field and the IMF can interconnect, and create open
33 magnetic flux, that consists of magnetic field lines that originate in the interior of the planet
34 and close through the interplanetary medium. The solar wind reaches the planet at a velocity
35 larger than the characteristic wave speed (the speed of magnetosonic waves), so that a bow
36 shock envelopes the magnetic environment of the planet, at a typical standoff distance of ~ 15
37 Earth radii (R_E) upstream from the planet in the subsolar region. The pressure exerted by the
38 solar wind on the Earth's magnetosphere compresses it on the dayside, and gives it an
39 elongated shape, creating the magnetotail on the nightside. Newly opened field lines, created
40 on the dayside, are convected antisunward towards the magnetotail where they eventually
41 undergo another reconnection process that closes them again, thus reconfiguring the magnetic
42 topology back to a more dipolar pattern, releasing the energy that regularly powers the
43 substorm expansion phase. Occasionally, the Sun releases a burst of material, creating a
44 discontinuity in the solar wind, that translates to an increased dynamic pressure, either due to
45 the increased plasma density or to an enhanced velocity (or both), the most spectacular of

46 which is the coronal mass ejection (CME), i.e. an explosive process that releases large
47 quantities of solar material into space. When a solar wind pressure front reaches the Earth, it
48 compresses the magnetosphere, and sometimes triggers a substorm expansion phase, during
49 which a large amount of open flux is closed in the magnetotail.

50 *Boudouridis et al.* [2003, 2004] showed that the interaction of the magnetosphere with
51 solar wind dynamic pressure pulse results in a sharp reduction in the polar cap size, a clear
52 signature of flux closure, especially when a pressure pulse hits the magnetosphere after an
53 interval of southward IMF, i.e. after the magnetosphere has been loaded with open flux by
54 magnetic reconnection on the dayside. *Brittnacher et al.* [2000] observed an auroral
55 intensification triggered by a CME which develops from the dayside oval and propagates
56 towards the nightside. *Meurant et al.* [2003, 2004] showed that solar wind dynamic pressure
57 pulses can trigger an enhancement of auroral activity, in agreement with *Boudouridis et al.*
58 [2003]. They showed that this enhancement is stronger for southward IMF conditions. For the
59 set of events studied by *Meurant et al.* [2004], the preconditioning of the magnetosphere was
60 found to be less important than the properties of the solar wind during the pressure pulse. In
61 particular, they found that the auroral response is stronger for larger IMF intensity and solar
62 wind speed. It was also shown that the propagation of the auroral brightening from the
63 dayside to the nightside occurred sooner for the proton aurora than for the electron aurora
64 [*Meurant et al.*, 2003]. Moreover, compression of the dayside magnetosphere first results in
65 the formation of a dayside subauroral proton flash [*Hubert et al.*, 2003]. It was also shown
66 that the compression of the magnetotail by a solar wind dynamic pressure pulse can also
67 directly stimulate magnetic flux closure because it creates the conditions necessary for
68 magnetic reconnection in the tail [*Hubert et al.*, 2006b] as the pressure disturbance propagates
69 all the way down to the plasma sheet. *Meurant et al.* [2005] showed that pressure pulse-
70 induced and isolated substorms largely share the same properties, the pulse being the trigger
71 that initiates the reconfiguration of the unstable magnetosphere.

72 We have developed a method that combines ground based data from the Super Dual
73 Auroral Radar Network (SuperDARN) and global images of the proton aurora from the
74 Spectrographic Imager at 121.8 nm (SI12) onboard the Imager for Magnetosphere to Aurora
75 Global Exploration (IMAGE) satellite [*Mende et al.*, 2000a, b] in order to estimate the
76 magnetospheric open flux and the opening and closure rates of magnetic flux [*Hubert et al.*,
77 2006a]. These rates are expressed as voltages according to Faraday's law.

78 In the present study, we analyse the relation between the properties of solar wind
79 pressure pulses and the magnetospheric response in terms of open flux storage and closure. In
80 particular, we search for correlations between the properties of the solar wind and the opening
81 and closure of magnetic flux. The configuration of the geomagnetic field is also considered
82 using geosynchronous data from the GOES satellites. The role of preconditioning of the
83 magnetospheric system is considered as well. Throughout the text, we will interchangeably
84 use the terms (solar wind) dynamic pressure front or pulse, pressure front or pulse, or simply
85 front or pulse to designate a solar wind dynamic pressure pulse.

86 2. Data Availability and Selection

87 As already outlined in the introduction, the amount of open flux is estimated using
88 data from the SI12 instrument of the FUV experiment onboard the IMAGE satellite [*Hubert*
89 *et al.*, 2006a]. This instrument produces global images of the Doppler shifted Lyman- α
90 emission, which is solely due to the precipitation of auroral protons, and is used here to
91 estimate the location of the open/closed field line boundary (ocb) at ionospheric altitude, as
92 well as its motion. The SuperDARN radar network measures the ionospheric convection, and
93 allows the reconstruction of the ionospheric electric field [*Ruohoniemi and Baker*, 1998;
94 *Cowley and Lockwood* 1992]. The SI12 data are used in combination with the SuperDARN
95 radar data to estimate the opening and closure voltages that characterise the variations of the
96 amount of open flux. The solar wind data are from the ACE satellite. We found 68 cases of
97 pressure pulses over the period from June 2000 to February 2002, for which ACE, SI12 and
98 SuperDARN data were available. Instead of identifying the pressure pulses from a criterion
99 based on variations of the solar wind dynamic pressure, we identified dynamic pressure pulses
100 from a more pragmatic standpoint. It has been shown that, when a solar wind pressure pulse
101 reaches the Earth, it compresses the dayside magnetosphere in such a manner that it
102 stimulates the precipitation of protons along closed field lines that map to the dayside
103 ionosphere at magnetic latitudes lower than that of the auroral oval, creating a dayside
104 subauroral proton flash [*Hubert et al.*, 2003; *Fuselier et al.*, 2004]. We searched the SI12
105 dataset for dayside subauroral proton flash signatures, and we checked a posteriori that there
106 was actually an increase of the solar wind dynamic pressure in the ACE solar wind data, when
107 available. This pragmatic approach also has the advantage of reducing the uncertainty in the
108 time of propagation of the solar wind feature from the ACE location to the Earth's
109 magnetosphere, especially if we consider that a shock wave (or any disturbance) propagates

110 within the medium in addition to being advected along with the plasma motion. Moreover, in
111 the case of weak pressure pulses, we can be sure that the solar wind pressure front did actually
112 interact with the magnetosphere. For these weak pressure pulses, the identification of the
113 pressure increase responsible for the proton flash was sometimes more difficult, and there
114 remains some uncertainty in a few cases. The method of selection of pressure pulse-events led
115 us to select more than 85 cases of dynamic pressure fronts. Some of them had to be excluded
116 because of a failure of our open/closed boundary identification software, especially when the
117 viewing conditions were not good enough or when the proton aurora was too dim, leaving us
118 with 68 cases.

119 The duration of the interval that we investigate after the arrival of a particular pressure
120 front is again determined from a pragmatic standpoint: the interaction of the pressure front
121 with the magnetosphere generally stimulates an intensification of the flux closure voltage
122 (sometimes minor). The end of the interval that we consider is chosen to be the time at which
123 the closure voltage returns to a value close to its initial level prior to the front arrival (i.e.
124 within 10 kV), with a maximum duration limited to 35 minutes. In exceptional cases when the
125 intensification of the closure voltage is so weak that it remains under 10 kV, a duration of 20
126 min is chosen. As an example, **Figure 1** shows the solar wind properties, the open flux, the
127 opening and closure voltages, and the net reconnection voltage obtained on 4 November
128 2000. As the nightside (dayside) reconnection voltage represents a decrease (an increase) of
129 the open flux, we choose to express the nightside flux closure (dayside flux opening) rate as a
130 negative (positive, respectively) voltage, so that the net voltage, i.e. the sum of the opening
131 and closure voltages, represents the time derivative of the open flux. A sharp dynamic
132 pressure front was observed by the ACE satellite shortly after 0130 UT. This front reached the
133 Earth and triggered a dayside subauroral proton flash detected by the SI12 instrument at 0224
134 UT (vertical dotted line). The open magnetic flux deduced from the SI12 observations prior to
135 the dynamic pressure pulse arrival was rather low (~ 0.46 GWb), a situation compatible with
136 the northward IMF orientation. The closure voltage estimated from the SI12 and SuperDARN
137 observations intensified after the dynamic pressure pulse arrived at the planet and reached \sim
138 125 kV. The closure voltage returned to pre-pulse values after ~ 35 min. Note that, as time
139 smoothing has to be applied to correctly estimate the reconnection voltages, in an absolute
140 sense, our resolution is not the cadence of image acquisition of the FUV-SI12 instrument (i.e.
141 ~ 2 min) but only ~ 12 -14 min. This results in a smearing of the pulse signature in the closure
142 voltage curve, so that the striking time coincidence between the very sharp signature in the

143 slope of V_{cl} and the pressure front arrival can be considered incidental: although the pressure
144 pulse arrival generally initiates an intensification of the flux closure, the signature in the
145 closure voltage curve is generally not that sharp right at the time of the arrival of the solar
146 wind dynamic pressure pulse.

147 Several quantities can be determined that, potentially, can reveal the nature of the
148 interaction between interplanetary shocks (dynamic pressure fronts in this study) and the
149 magnetosphere. The amount of open flux itself is of course considered, but its variations can
150 also be important: the net variation of the open flux, its maximum rate of change during the
151 whole event and during the interaction of the magnetosphere with the ramp of the solar wind
152 pressure front, and its initial value are all physical quantities to be studied as well. A similar
153 study of the flux closure rate can also be undertaken: its average, initial, and maximal values
154 must be considered (maximum in terms of its absolute value, i.e. the minimal value of the
155 closure voltage, which is a negative number). The net intensification and rate of change of
156 the closure voltage has also to be considered. In addition, the time integral of the closure
157 voltage is also computed. It represents the total amount of open flux that goes through closure
158 during the interval, whereas the variation of the amount of open flux during the interval
159 includes a flux opening contribution from the dayside reconnection site.

160 The solar wind data can also be used to determine several parameters that can,
161 possibly, play an important role in the interaction between solar wind dynamic pressure pulses
162 and the magnetosphere. The most natural parameter to be considered is obviously the solar
163 wind dynamic pressure itself (P_{dyn}). Previous studies mentioned in section 1 above [*Meurant*
164 *et al.*, 2003, 2004] have however shown that this may not be the most important parameter.
165 We will nevertheless consider this parameter, as well as its variation (maximum value,
166 pressure jump, rate of change etc) for correlation with the magnetospheric response expressed
167 in terms of open flux, closure voltage etc. The second natural parameter is the solar wind
168 velocity (v_{sw}), that has already been pointed out as a key parameter governing the
169 magnetospheric response to a solar wind pressure pulse. The solar wind density (n_{sw}) is also
170 considered, but these three solar wind properties are not independent, as $P_{dyn} = n_{sw} m v_{sw}^2$. The
171 interplanetary magnetic field (IMF : B_{sw}) has also to be studied, not only its magnitude, but
172 also the value of each component, and their variations. The solar wind properties can be
173 combined according to the model of *Petrinec and Russell* [1993, 1996], to estimate the size of
174 the magnetospheric cavity: the “radius” of the magnetopause R_M (i.e. the distance between the

175 dayside nose of the magnetopause and the planet), the radius at $x_{GSM} = 0$ and its cross section
176 may be important, as well as the variations of these quantities. The standoff distance of the
177 bow shock R_B can also be treated in a similar manner.

178 We also consider the magnetospheric response in terms of its signature at
179 geosynchronous altitude. More specifically, the elevation angle of the magnetic field is
180 studied on the nightside using data from the GOES-8 satellite. These data are available only
181 for a subset of events, so that less accurate results may be obtained.

182 We anticipate the next sections by summarizing in **Table 1** the quantities that will be
183 actually discussed in this paper and their definition. In this study, the time interval reported in
184 **Table 1** is that of the pressure pulse-induced flux closure. More variables and correlation
185 pairs were considered initially, but we will focus on the ones we found to be the most
186 interesting. Several variables specifically deal with the ramp of the dynamic pressure front.
187 The front ramp is determined as follows: the time derivative of the solar wind pressure is
188 computed using a Savitzky-Golay filtering [*Savitzky and Golay, 1964*], and the time interval
189 of increasing dynamic pressure around the time of maximum derivative is considered as the
190 ramp of the pressure front. This concept is however a bit loosely defined in the case of a very
191 weak pressure pulse. The Savitzky-Golay smoothing filter can be used to smooth a noisy
192 signal. The filter is defined as a weighted moving average with weighting given as a
193 polynomial of a certain degree. The returned coefficients, when applied to a signal, perform a
194 polynomial least-squares fit within the filter window. This polynomial is designed to preserve
195 higher moments within the data and reduce the bias introduced by the filter, and the
196 derivatives of the smoothed signal can be obtained.

197 3. Statistical Analysis

198 The variables discussed in Section 2 have been searched for correlation. A set of 68
199 solar wind dynamic pressure pulse events has been identified in the SI12, SuperDARN and
200 ACE datasets, and treated to estimate the open flux, reconnection voltages, dynamic pressure
201 etc of these intervals. The method outlined above is applied to determine the duration of each
202 pulse interval. Correlations are searched for between the geomagnetic quantities (open flux,
203 voltages, elevation angle etc, and their variations) and solar wind properties. The correlation
204 is studied using both Fisher's test and the Student test. The significance level of the
205 correlations are obtain in the sense of bilateral tests, and the critical level of confidence is
206 such that the estimated Pearson correlation coefficient equals one of the limit of the test

207 interval that brackets correlation cases undistinguishable from the case $r = 0$. For the student
208 test, the quantity $\frac{\hat{r} \sqrt{n-2}}{\sqrt{1-\hat{r}^2}}$ (\hat{r} being the estimated correlation coefficient) is known to follow
209 a t_{n-2} distribution function under the $r = 0$ hypothesis, which allows bilateral testing. In the
210 case of the Fisher test, the quantity $z = \frac{1}{2} \ln\left(\frac{1+\hat{r}}{1-\hat{r}}\right)$ is calculated, which is known to follow a
211 Gaussian distribution $N\left(\frac{1}{2} \ln\left(\frac{1+r}{1-r}\right), \frac{1}{\sqrt{n-3}}\right)$ which again allows us to perform a bilateral
212 testing under the $r = 0$ hypothesis. Whatever the test used, the (critical) level of confidence
213 tells us how confident we should feel that the estimated correlation coefficient differs from
214 zero, whereas the square of the correlation coefficient (also called the coefficient of
215 determination) tells us what fraction of the variance of the dataset could be explained by the
216 dependence of both data on each other. From a mathematical standpoint, the Fisher test is
217 known to be inefficient for small size samples (less than ~ 25 data pairs), whereas the Student
218 test is always valid. Clearly, both tests give different significance levels for a given sample,
219 but both significance levels tend to the same limit as the sample size is increased. Obviously,
220 if n tends to infinity, one is supposed to reach absolute certainty and the significance level is
221 always 1, whatever the test used. (In the following paragraphs, we will use the symbol r
222 instead of \hat{r} .) In our study, both tests give very similar results. More than 1200 pairs of
223 variables were considered. A very large number of these pairs were found to be (linearly)
224 correlated under a level of confidence of 0.9. Clearly, much higher levels of confidence must
225 be used to identify the correlation. The critical level of confidence was determined for each
226 pair of variables (i.e., the level of confidence under which the correlation coefficient of the
227 considered pair of variables is equal to the threshold value that discriminates between
228 correlated and uncorrelated variables, i.e. between non-zero and zero correlation coefficient).
229 From a mathematical standpoint, it is impossible to define an absolute threshold that
230 discriminates once and for all between correlated and uncorrelated samples of paired
231 variables. Only a hypothesis test can be carried out and the significance of a correlation must
232 be expressed in terms of a level of confidence. The significance is however not the final word,
233 as a low correlation can be statistically significant, and the square of the correlation
234 coefficient can be used as a measure of the part of the variations in the dataset that can be
235 explained by the dependence between the correlated variables. In this study, we will
236 essentially present the most significant correlations. The critical level of confidence can be

237 estimated according to Fisher's or Student's test. We will always quote the worst of these
238 two. For every variable, outliers are systematically eliminated: data points such that $|x_i -$
239 $m| > 3\sigma$ are rejected, with m the average value of the ensemble $\{x_i\}$, and σ the standard
240 deviation of the sample. One can consider that this is a rather conservative choice that tends to
241 reduce the inferred correlations, because in a collection of sets of 68 data points, an average of
242 ~ 0.18 points per sample would fall outside of the $|x_i - m| > 3\sigma$ interval, assuming a Gaussian
243 distribution of the data, so that one can expect that a data point representative of the natural
244 distribution may be found outside of the selected interval in $\sim 20\%$ of the cases.

245 **Figure 2** shows the distribution function of several properties of the solar wind for our
246 set of events. The dotted lines show the distribution function and a smoothing is applied to
247 produce the solid lines. The average (m) and standard deviation (σ) of the sample are also
248 given. The bin size used to construct a distribution function is $10 \times \sigma/\tilde{n}$ with \tilde{n} the number of
249 points of the sample found in a 2σ - wide interval centred on m . The dynamic pressure increase
250 across the pressure front is shown in the top panel. It clearly appears that most of the fronts
251 included in this study were rather weak: the median of the distribution is 3 nPa. This also
252 appears in the solar wind density increase across the pressure pulse (middle panel) with a
253 median value of 9.15 cm^{-3} and a most probable value of $\sim 4 \text{ cm}^{-3}$. The variation of the solar
254 wind speed across the dynamic pressure discontinuity (third panel) is generally positive,
255 although the most probable value is $\sim 0 \text{ km/s}$. Indeed, as the dynamic pressure is proportional
256 to the square of the velocity, a small increase of the velocity will produce a large increase of
257 the dynamic pressure (a 10% increase of the velocity produces a 20% increase of the dynamic
258 pressure).

259 Considering the net open flux budget, the value of the open flux at the end of the
260 pressure pulse-induced flux closure (Φ_{final}) is, first of all, correlated with the open flux
261 available prior to the pressure front arrival (Φ_{init}) (**Figure 3, Table 2**). The correlation
262 coefficient is $r = 0.807$, and the correlation hypothesis must be accepted with a confidence
263 level better than $\alpha = 0.999$ (according to both Fisher and Student tests). (Throughout this
264 paper, we will denote a correlation coefficient with the symbol r , and a level of confidence
265 with the symbol α .) This correlation can account for $r^2 = 0.65$ (65%) of the observed variance,
266 so that much larger correlations must not be expected with other parameters, and Φ_{init} is
267 considered here as one of the independent variables. Indeed, the value of Φ_{init} results from the
268 past history of the solar wind – magnetosphere interaction and represents a preconditioning of

269 the system. As may be expected, the final open flux also correlates with the IMF B_z . The Φ_{final}
 270 and $B_{z,max}$ (generally positive) are anticorrelated (accounting for ~17% of the variance only)
 271 (**Table 2**). This can be easily understood: when the IMF is northward, very little open flux can
 272 be created on the dayside, and the open flux is then lower. The relation between the IMF B_z
 273 component and the creation of open flux is already well known, so we will not dwell on this
 274 subject. The final amount of open flux also anticorrelates with the maximum value of P_{dyn} ,
 275 $P_{dyn,max}$ and with the pressure jump (ΔP_{dyn}). Strong compression of the tail thus favours lower
 276 values of Φ_{final} , but the amount of open flux itself depends more on the past history of the
 277 magnetosphere through Φ_{init} , both correlations with $P_{dyn,max}$ and ΔP_{dyn} being able to account
 278 for ~9% of the variance only.

279 The variation of the open flux ($\Delta\Phi$), which results from the balance between flux
 280 opening on the dayside and flux closure in the tail, and the amount of flux closed during the
 281 event (i.e. $\Phi_{cl} = \int_{t_0}^{t_1} V_{cl} dt$ with V_{cl} the closure voltage and $[t_0, t_1]$ the considered time interval)
 282 may be quantities much more representative of the magnetosphere – pressure front interaction
 283 rather than the amount of open flux itself. However, the best correlation for both quantities is
 284 found with Φ_{init} as well (**Figure 4, Table 3**) explaining 16-17% of the variance. Indeed,
 285 $\Delta\Phi = \Phi_{final} - \Phi_{init}$ and Φ_{final} already correlates with Φ_{init} . Also, Φ_{cl} represents the amount of
 286 open flux that goes through reconnection and, if the amount of open flux newly created on the
 287 dayside during the considered interval is not too large, Φ_{cl} cannot be larger than Φ_{init} . But this
 288 correlation nevertheless suggests that, as the magnetosphere accumulates open flux, its ability
 289 to close flux in the tail under the stimulation of a pressure pulse is increased ($\Delta\Phi$ and Φ_{cl} are
 290 negative numbers). The importance of magnetospheric preconditioning also appears in the
 291 correlation of $\Delta\Phi$ and Φ_{cl} with the maximum value of the magnetopause radius (the standoff
 292 distance of the magnetopause) $R_{M,max}$ computed based on solar wind data using the model of
 293 *Petrinec and Russell* [1993, 1996], both being able to explain ~10% of the variance. Similar
 294 correlations are also found with the standoff distance of the bow shock $R_{B,max}$ and with the
 295 initial values of R_M and R_B : $R_{M,init}$ and $R_{B,init}$, with slightly lower confidence.

296 These correlations suggest that the magnetospheric preconditioning is not limited to
 297 the accumulated open flux, but also includes the cross section of the magnetospheric cavity
 298 exposed to the solar wind flow, the standoff distance being considered here as a rough proxy
 299 describing the shape of the magnetosphere. In the model of *Petrinec and Russell* [1993,

300 1996], the standoff distance of the magnetopause is a complicated non-linear function of both
 301 B_z and P_{dyn} , and one may wonder if the correlation with the magnetopause radius does not
 302 stem from a correlation with P_{dyn} , especially with its initial value, or with its variation across
 303 the dynamic pressure front. In our sample, which includes weak pulses, we found that the
 304 dynamic pressure does not seem to strongly drive the flux closure process, as we will show
 305 below. It can also be noted that Φ_{op} , the amount of open flux created on the dayside during the
 306 pressure pulse-induced flux closure interval, and Φ_{cl} do not well correlate with each other
 307 (**Table 3**), suggesting that tail reconnection closes accumulated open flux rather than newly
 308 opened flux. Neither is a significant correlation found between Φ_{op} and $\Delta\Phi$. This supports the
 309 importance of the loading-unloading paradigm, in which open magnetic flux and energy are
 310 accumulated in the tail before intense flux closure can begin, compared with the direct driving
 311 of the magnetosphere by the solar wind [*Blockx et al., 2009*, and references therein] in which
 312 new magnetic energy is supplied through the tail magnetopause and is nearly immediately
 313 available for dissipative processes. Indeed, the transport of magnetic flux from the dayside
 314 magnetopause to the nightside reconnection site can take of the order of one hour. It is no
 315 surprise, however, that Φ_{op} is well correlated with $B_{z,min}$ ($r = -0.437$, $\alpha = 0.999$) as a
 316 southward IMF (i.e. a negative IMF B_z) is a condition that strongly stimulates magnetic
 317 reconnection on the dayside.

318 The value of the flux closure voltage itself basically correlates with Φ_{init} (**Figure 5**,
 319 **Table 4**): the average reconnection voltage $\overline{V_{cl}}$ has its best correlation with Φ_{init} ($r^2 \sim 21\%$).
 320 $\overline{V_{cl}}$ then correlates with $R_{M,max}$ and $R_{B,max}$ ($r^2 \sim 17\%$). The median voltage computed during
 321 the considered time interval, $\underline{V_{cl}}$, has its best correlation with Φ_{init} , then with $R_{M,max}$ and $R_{B,max}$
 322 possibly representing $\sim 16-17\%$ of the variance. (Note that $R_{M,max}$ and $R_{B,max}$ are not
 323 independent on each other). Slightly lower correlations are again found with $R_{M,init}$ and $R_{B,init}$
 324 (**Figure 5, Table 4**). These correlations show that the preconditioning of the magnetosphere is
 325 important for the process of flux closure itself. These results do not really differ from those
 326 presented for Φ_{cl} , as in principle, $\Phi_{cl} = \overline{V_{cl}} \Delta t$, with Δt the duration of the pressure pulse-
 327 induced flux closure interval. (Note that, in our study, Φ_{cl} is not exactly equal to $\overline{V_{cl}} \Delta t$
 328 because Φ_{cl} is obtained from a numerical integration, whereas $\overline{V_{cl}}$ is the simple arithmetic
 329 average of the discrete series of closure voltage values. This choice was made to ease the
 330 comparison between $\overline{V_{cl}}$ and $\underline{V_{cl}}$, whereas Φ_{cl} has to be compared with $\Delta\Phi$.)

331 The minimum value reached by the closure voltage $V_{cl,min}$ represents the maximum
332 rate of flux closure, because V_{cl} is a negative number. This quantity best correlates with $R_{M,max}$
333 and $R_{B,max}$ ($r^2 \sim 17\%$) (**Table 5**). Similar correlations are found with $R_{M,init}$ and $R_{B,init}$, which,
334 naturally, are close to $R_{M,max}$ and $R_{B,max}$, respectively. Solar wind properties correlate slightly
335 better with $V_{cl,min}$ than Φ_{init} . The variation of the IMF intensity $\Delta|B|$ correlates with $V_{cl,min}$ as
336 well as its average rate of change during the dynamic pressure front ramp $\left. \frac{d|B|}{dt} \right|_{ramp}$ and the
337 variation of the solar wind velocity across the ramp of the pressure pulse $\Delta v_{sw}|_{ramp}$. These last
338 correlation coefficients remain weak. (All these correlations can account for 10-12% of the
339 variance). The solar wind dynamic pressure does not seem to play a significant role so far in
340 the analysis of the sample of dynamic pressure pulse-induced flux closure presented here
341 (although the dynamic pressure and the solar wind velocity are dependant quantities).

342 The only potential-related parameter that we find to be well correlated with one of the
343 solar wind properties is the intensification of the closure voltage $\Delta V_{cl} = V_{cl,max} - V_{cl,init}$, the
344 difference between the maximum and initial closure voltage as determined on the basis of
345 SI12 and SuperDARN observations. ΔV_{cl} correlates best with $\Delta|B|$ and with $\Delta v_{sw}|_{ramp}$ (**Table**
346 **6**). These correlations can represent only $\sim 9-12\%$ of the observed variances. The level of
347 confidence of these correlations is somewhat lower than the values presented above, that had
348 levels of confidence reaching 0.999. An increase in the modulus of B, as well as an increase
349 of the velocity implies an increase of the electric field of the solar wind, which is the cross
350 product of the velocity and magnetic field (we exclude here the improbable situation in which
351 the increase of $B - v -$ would only take place along the component parallel to $\vec{v} - \vec{B}$,
352 respectively $-$). One can here wonder if a possible penetration of the interplanetary electric
353 field into the magnetosphere can significantly influence the process of magnetic reconnection.
354 This might be supported by the fact that the best correlation of ΔV_{cl} is found with Φ_{op} which,
355 in principle, is proportional to the electric field in the solar wind, whereas we have seen above
356 that the magnetosphere essentially closes a part of the accumulated open flux rather than the
357 newly opened flux.

358 Inspection of the correlations found between the solar wind properties and the
359 quantities representative of the closure process suggests that the pressure fronts of our dataset
360 rather had the effect of initiating the flux closure process, which was controlled by the

361 properties of the magnetosphere. Indeed, the flux closure is not strongly correlated with the
 362 pressure jump. To a first approximation it does not depend on the properties of the solar wind
 363 pressure front, but rather on the initial state of the magnetosphere. Clearly, if independent
 364 parameters had to be selected as the main variables that control the compression-induced flux
 365 closure process, one could select Φ_{init} and $R_{M,max}$ in the first place, possibly supplemented by
 366 $\Delta|B|$ and $\Delta v_{sw}|_{ramp}$. The dynamic pressure discontinuity is rather presented here as a trigger that
 367 favours the growth of some instability of the magnetosphere and, more specifically, of the
 368 plasma sheet, that eventually ends in a relaxation of the whole system through flux closure,
 369 that reconfigures the field of the magnetotail. **Figure 6** shows the lack of correlation (**Table**
 370 **7**) between the dynamic pressure increase ΔP_{dyn} and the closure voltage intensification ΔV_{cl}
 371 (**Figure 6a**) and the closed flux Φ_{cl} (**Figure 6b**). The dispersion of the full dataset is such that
 372 no significant correlation can be found. However, **Figure 6a** also suggests that a subset could
 373 be isolated for $\Delta P_{dyn} > \sim 2.8$ nPa (the method used to determine this threshold is explained in
 374 the next section: it corresponds to an optimal correlation). The dotted vertical lines in **Figure**
 375 **6a,b** isolate this subset, and the solid lines are the least absolute deviation fits through the
 376 data. For the subset, higher correlation coefficients are found for ΔV_{cl} and Φ_{cl} with ΔP_{dyn}
 377 (**Table 7**), representing nearly 25% of the variance. This suggests on statistical grounds that a
 378 sufficiently strong solar wind dynamic pressure pulse can directly influence the flux closure
 379 process. Indeed, a previous study of *Hubert et al.* [2006b] showed that a strong compression
 380 of the tail can actively stimulate the flux closure process in the plasma sheet. Considering the
 381 distribution function of ΔP_{dyn} in **Figure 2**, it clearly appears that most of the pressure fronts
 382 included in our dataset were weak ones, and one could wonder if weak and strong pressure
 383 pulses have the same impact on the magnetosphere. Indeed, it may seem surprising that the
 384 defining parameter of an interplanetary pressure front does not influence at all the response of
 385 the magnetosphere to a pressure pulse.

386

387 4. Subset Statistics

388 As the properties of the solar wind pressure fronts in our dataset do not appear to
 389 significantly influence the magnetospheric response expressed in terms of flux closure, we
 390 conducted an analysis aimed at identifying subsets in the dataset for which a better correlation
 391 is found between the flux closure-related parameters and the solar wind-related parameters.
 392 The quality of the correlation is not determined by the value of the correlation coefficient

393 itself, but rather by the level of confidence in the correlation, which combines the correlation
394 coefficient and the number of observations available in the (sub)sample. Outliers are rejected
395 from the analysis by applying the same procedure to the subset of data as that described above
396 for the full dataset.

397 It has been possible to find thresholds on various dynamic pressure-related parameters
398 that isolate subsets of events for which a correlation is found with the variables describing the
399 response of the magnetosphere in terms of flux closure. We propose to use these thresholds to
400 quantify what can be considered as a strong solar wind dynamic pressure pulse, i.e. a pulse
401 that causes a magnetospheric response sensitive to the dynamic pressure itself. All things
402 considered, identifying dynamic pressure fronts implicitly assumes that dynamic pressure
403 variations can be classified into two categories: modest variations on the one hand, and pulses
404 on the other, without proposing a well defined criterion allowing us to discriminate between
405 them. In our dataset selection, we chose to classify dynamic pressure variations as fronts if
406 they produce a dayside subauroral proton flash, to be detected in the SI12 images. This
407 criterion makes sense because the dayside subauroral proton flash is a natural signature
408 indicating a sudden compression of the dayside magnetosphere by the solar wind. Nothing
409 guarantees, however, that this dayside-based criterion allows us to fully appreciate the nature
410 of a dynamic pressure variation in terms of the nightside response of the magnetosphere to a
411 dynamic pressure front.

412 Pressure fronts presenting a solar wind dynamic pressure increase ΔP_{dyn} larger than
413 ~ 2.8 nPa form a subset for which ΔP_{dyn} and ΔV_{cl} correlate well, so that their interdependence
414 could account for $\sim 25\%$ of the variance of the subsample (**Figure 7, Table 8**). This clearly
415 expresses a reaction of the magnetosphere in response to the dynamic pressure increase in
416 terms of an intensification of the flux closure rate. The same threshold value of ~ 2.8 nPa was
417 found when searching for the best possible correlation between ΔP_{dyn} and $V_{cl,min}$ but the
418 correlation coefficient was found to be rather low, as well as the level of confidence. Finding
419 the same threshold for these two parameters is not surprising, as they are not independent of
420 each other. It nevertheless suggest that, for strong pressure fronts, the solar wind dynamic
421 pressure partly controls the process of flux closure in the tail by compressing it, as explained
422 in *Hubert et al.* [2006b]. Variable Φ_{cl} is found to have a better correlation with ΔP_{dyn} for a
423 threshold of ~ 2.8 nPa as well, the correlation accounting for $\sim 12\%$ of the variance, while $\overline{V_{cl}}$
424 and $\overline{V_{cl}}$ are both found to better correlate with ΔP_{dyn} for a threshold of ~ 3 nPa. The threshold

425 for correlation with $\Delta\Phi$ is 2.8 nPa as well, but the correlation coefficient is very low. A
426 reasonable threshold to discriminate between strong and weak pressure pulses based on the
427 dynamic pressure increase across the dynamic pressure jump could therefore be chosen as
428 $\sim 2.8 - 3$ nPa. This value of the pressure increase can be compared with the typical value of
429 the solar wind dynamic pressure, i.e. 3 nPa [*Feldman, 1977*]. Not surprisingly, a threshold
430 could also be found for the maximum rate of change of the dynamic pressure $\left. \frac{dP_{dyn}}{dt} \right|_{\max}$ (**Table**
431 **9**). A maximum level of confidence on correlation is found for this parameter with ΔV_{cl}
432 ($r^2 \sim 34\%$), Φ_{cl} ($r^2 \sim 24\%$), $\overline{V_{cl}}$ ($r^2 \sim 14\%$) and $V_{cl,min}$ ($r^2 \sim 22\%$) for a threshold value of
433 $\left. \frac{dP_{dyn}}{dt} \right|_{\max} > 2.14 \times 10^{-2}$ nPa/s, whereas a threshold of 1.80×10^{-2} nPa/s gives a maximum level
434 of confidence for correlation with $\underline{V_{cl}}$ ($r^2 \sim 12\%$) and $\Delta\Phi$ ($r^2 \sim 6\%$, this value being rather
435 low). A typical threshold could be chosen based on these results, but the dynamic pressure
436 growth has also to last for a sufficiently long time to produce a significant pressure increase.

437 The closure voltage intensification ΔV_{cl} and the total amount of flux closed Φ_{cl} are also
438 found to be well correlated with the maximum dynamic pressure reached during the pressure
439 pulse-induced flux closure interval P_{max} (**Figure 8, Table 10**), restricting the dataset to events
440 with $P_{max} > 5.97$ nPa ($r^2 \sim 28\%$; $r^2 \sim 11\%$ respectively). Maximum levels of confidence on
441 correlation are found between P_{max} and $V_{cl,min}$, $\underline{V_{cl}}$ and $\overline{V_{cl}}$ when restricting to $P_{max} > 6.14$ nPa,
442 with poorer correlation however ($r^2 \sim 12\%$; $r^2 \sim 7\%$; $r^2 \sim 7\%$ respectively). A reasonable
443 threshold for a strong pressure pulse could thus be chosen as $P_{max} > 6$ nPa, but the net change
444 of dynamic pressure must nevertheless be considered as well, as shown above, because the
445 solar wind can present intervals of steady high dynamic pressure. Indeed, the dependence on
446 P_{max} is not able to account for much of the variance of the studied subsets.

447 Variations of the solar wind velocity are not only associated with variations of the
448 electric field in the solar wind, they are also able to produce strong variations of the dynamic
449 pressure. Both effects could influence the process of magnetic flux closure in the tail. Indeed,
450 ΔV_{cl} and $\Delta v_{sw}|_{ramp}$, the variation of the solar wind velocity during the ramp of the dynamic
451 pressure front, are strongly correlated ($r^2 \sim 34\%$) = -0.586, $\alpha = 0.9997$) if the analysis is
452 restricted to events with $\Delta v_{sw}|_{ramp} > 11.3$ km/s (**Figure 9, Table 11**). The correlation is even

453 better with the other variables related with the closure voltage, the correlation being able to
454 account for 53% of the variance of \underline{V}_{cl} . It clearly appears that an increase of the solar wind
455 velocity by more than 11-12 km/s during the ramp of the dynamic pressure front causes a
456 stronger response of the magnetosphere in terms of flux closure.

457 Very similar results are obtained concerning the variation of the solar wind velocity
458 across the whole interval considered ($\Delta v_{sw} = v_{sw,max} - v_{sw,init}$), but with a threshold value of
459 ~ 8.6 km/s, i.e. roughly 25% lower than the threshold obtained for $\Delta v_{sw}|_{ramp}$ (**Table 12**). This
460 difference could however be due to the fact that $\Delta v_{sw} \geq \Delta v_{sw}|_{ramp}$, which can slightly modify
461 the correlations. As this threshold is independent of the manner in which the ramp is defined,
462 it may finally be a more suitable threshold. One could argue that a 12 km/s increase in the
463 solar wind velocity can take place progressively during a long interval, and should not be
464 considered a pulse. Indeed, we could also identify threshold values for the maximum rate of
465 change of the solar wind velocity. All thresholds found were larger than 0.22 km/s². A more
466 typical value could be ~ 0.286 km/s² (**Table 13**).

467 Considering the full dataset, it has been found above that a variation of the IMF
468 intensity influences the flux closure process in the tail, from a statistical standpoint. Keeping
469 the subset of events for which $\Delta|B| > 0.47$ nT (**Table 14**), one finds much better correlations
470 for ΔV_{cl} , $V_{cl,min}$, Φ_{cl} , \overline{V}_{cl} and \underline{V}_{cl} . Indeed, this nearly zero threshold value suggests that, in
471 fact, an increase of the IMF magnitude favours the process of dynamic pressure pulse-induced
472 flux closure. Further studies should elucidate if this is specific to the pulse-induced flux
473 closure, or if this is a general trend including flux closure intervals unrelated to a dynamic
474 pressure front.

475

476 The last paragraphs indicate that strong solar wind dynamic pressure pulses can be
477 defined, from the standpoint of their implication on the process of flux closure, as pressure
478 fronts presenting the following characteristics: a dynamic pressure increase of ~ 3 nPa, and/or
479 a dynamic pressure reaching ~ 6 nPa, and/or a velocity increase by some ~ 10 km/s. Events
480 combining these three properties should naturally be expected to be very efficient at directly
481 stimulating flux closure in the magnetotail. In addition, an increase of the IMF magnitude is

482 also a factor that favours a more intense closure voltage, but this is not necessarily specific to
 483 pressure pulse-induced flux closure intervals and should be checked by further studies.

484 The predominant importance of variations of the solar wind velocity can be
 485 highlighted by a full analysis of the subset defined by $\Delta P_{dyn} > 2.8$ nPa. For this subset, the
 486 variation of the solar wind velocity is found to be the one that best correlates with ΔV_{cl} , $V_{cl,min}$,
 487 Φ_{cl} , $\overline{V_{cl}}$ and $\underline{V_{cl}}$ (**Table 15, Figure 10**), the correlations explaining between 30 and 46% of
 488 the variations. The correlation between the variation of the solar wind velocity and the
 489 parameters describing the pressure pulse-induced flux closure is obvious. It must be noted that
 490 the preconditioning by the accumulated open flux prior to the pulse arrival at Earth plays now
 491 a minor role. Indeed, Φ_{init} correlates with Φ_{cl} with $r = -0.318$ and $\alpha = 0.955$ only. All other
 492 correlations between Φ_{init} and the variables listed here are poorer. Clearly, a small correlation
 493 remains, especially with Φ_{cl} , because the amount of available open flux limits the amount of
 494 flux that can go through closure, but for strong pressure pulses, this remains a minor factor
 495 compared with the solar wind properties. It must be noted that ΔP_{dyn} correlates significantly
 496 with ΔV_{cl} ($r = -0.483$, $\alpha \sim 0.997$), whereas no other voltage-related parameter correlates well
 497 with ΔP_{dyn} . This suggests that, for strong pressure fronts, the compression of the
 498 magnetosphere leads to an intensification of magnetic reconnection without determining the
 499 value of the reconnection rate itself. The other voltage-related parameters better correlate with
 500 parameters related with the solar wind velocity: Δv_{sw} , as explained above but also $\Delta v_{sw}|_{ramp}$,
 501 $\frac{dv_{sw}}{dt}|_{max}$ etc. Another parameter that appears in the correlation analysis is the radius of the
 502 magnetopause at $x_{GSM} = 0$, i.e. at Earth location (ΔR_{M-E} , not listed in table 1). Its associated
 503 correlation coefficients, ranging between 0.45 and 0.56, are generally lower than those found
 504 for the velocity-related parameters. The magnetospheric radius can be found at any x_{GSM}
 505 using a proxy based on the solar wind properties [*Petrinec and Russell, 1993, 1996*] and is
 506 dependant on the solar wind velocity, the interplanetary magnetic field etc. ΔR_{M-E} can be
 507 viewed as a proxy for the compression of the magnetosphere that only depends on the solar
 508 wind properties, and these correlations show again the compression of the tail favours flux
 509 closure. If a set of independent variables that contribute to determine the magnetospheric
 510 response to strong solar wind dynamic pressure discontinuities had to be selected, one could
 511 probably choose Δv_{sw} and ΔP_{dyn} in the first place, possibly supplemented by ΔR_{M-E} , but it

512 would not be necessary to include the magnetospheric preconditioning, in contrast with the
513 results found for the full dataset.

514 5. Correlations with Geosynchronous Data

515 For a restricted subset of events, the GOES-8 satellite was located in the midnight
516 sector, which we consider here as a 6 h MLT interval centred on midnight MLT. We obtained
517 24 events satisfying that requirement. The elevation angle of the magnetic field measured at
518 geosynchronous altitude by the GOES-8 satellite, as well as its variations, was compared with
519 the results obtained from the SI12 and SuperDARN data to describe the open flux and the
520 closure voltage.

521 The open flux Φ_{init} accumulated prior to the solar wind dynamic pressure front arrival
522 is correlated with the initial (prior to the front arrival) value of the elevation angle e_{init} ($r = -$
523 0.762 , $\alpha = 0.998$, **Figure 11**). This is not surprising, considering that both quantities describe
524 two different aspects of the state of the magnetosphere, which as a whole results mainly from
525 its past interaction with the solar wind. The open flux accumulated by the magnetosphere can
526 be seen as the set of flux tubes that originate in the ionosphere and close through the
527 interplanetary medium. The accumulation and variation of the open flux results from the
528 imbalance at “short” time scales (typically ~an hour, i.e. the time scale of the substorm cycle)
529 between the flux opening on the dayside and flux closure in the tail. As the magnetosphere is
530 accumulating open flux, open flux tubes are dragged downtail by the motion of the solar
531 wind, which eventually produces a stretching of the tail, until open flux gets closed by
532 magnetic reconnection reducing both the stretching (return flow of the flux tubes) and the
533 amount of open flux. Both quantities, open flux and tail stretching expressed here in terms of
534 geosynchronous elevation angle, thus evolve in a dependant manner and will, to some extent,
535 be correlated. The natural consequence is that we should expect the flux closure process and
536 the elevation angle to be partly related to each other.

537 The minimum value of the closure voltage $V_{cl,min}$ which represents the extreme rate of
538 flux closure, is correlated with the minimum rate of change of the geosynchronous elevation
539 angle $\left. \frac{de}{dt} \right|_{min}$ ($r = 0.510$, $\alpha = 0.992$ –Fisher test-; $\alpha = 0.985$ –Student test- , **Figure 12**). A
540 reduction of the elevation angle is the signature of a change of the geomagnetic field to a less
541 dipolar configuration, so that its rate of change during a flux closure interval can be expected
542 to be positive. On the other hand, the compression of the tail by the solar wind dynamic

543 pressure pulse can be expected to produce a less dipolar configuration by moving the tail
 544 plasma towards the plasma sheet, together with the frozen-in magnetic field lines that it hosts,
 545 thus producing a decrease of the elevation angle. From that standpoint, $\left. \frac{de}{dt} \right|_{\min}$ can be seen as a
 546 proxy for the extreme rate of change of the magnetic field towards a compressed, less dipolar,
 547 configuration. We thus find that the extreme rate of flux closure is correlated with a proxy
 548 that, in the case of the interaction of the magnetosphere with a dynamic pressure front in the
 549 solar wind, describes the extreme rate of compression of the tail. The correlation that we find
 550 suggests that a sharper compression of the tail leads to a stronger extreme rate of flux closure.
 551 However, ΔV_{cl} and the variation of the elevation angle during the ramp of the solar wind
 552 dynamic pressure front Δe_{ramp} are negatively correlated ($r = -0.453$, $\alpha = 0.981$ -Fisher test-;
 553 $\alpha = 0.970$ -Student test- , **Figure 11**), showing that on a slightly longer time scale, the closure
 554 voltage intensification dominates the dynamics of the magnetospheric topology and
 555 configuration, driving it towards a more dipolar shape. It follows that, in the case of strong
 556 solar wind dynamic pressure pulses, the direct compression of the tail (expressed in terms of
 557 the extreme rate of decrease of the elevation angle) causes a transient stimulation of the flux
 558 closure: the stronger the compression, the stronger the extreme value of the closure rate, but it
 559 must be stressed that the negative value of $\left. \frac{de}{dt} \right|_{\min}$, which is a value obtained punctually at a
 560 given time of the pressure front interval, does not preclude the geomagnetic field from
 561 undergoing a global dipolarization on longer time scales during that interval. Nor does this
 562 result preclude other parameters from influencing the closure process, but it stands along the
 563 same lines as the results from *Hubert et al.* [2006b] who also showed that a pressure front can
 564 drive transient flux closure by direct compression of the magnetotail down to the plasma
 565 sheet. The first consequence of a compression of the tail is an increase of the current density
 566 within the plasmashet. If we note L the characteristic scale of the magnetospheric cavity,
 567 which is reduced by the compression, then the conservation of magnetic flux during the
 568 compression implies that the magnetic field strength (B) increases proportionally to $\sim 1/L^2$. In
 569 addition, the width of the plasma sheet (w) can be expect to decrease proportionnaly to $\sim L^{1.4}$
 570 (approximately, for an adiabatic compression to match the field pressure in the lobes), so that
 571 the current density, which is roughly proportionnal to $2B/w$, increases according to $\sim 1/L^{3.4}$. If
 572 the characteristic scale can be expected to vary roughly proportionnally to $P_{\text{dyn}}^{-1/6}$ [*Kivelson*
 573 *and Russell, 1997*], then the current density can be expected to vary proportionnally to
 574 $\sim P_{\text{dyn}}^{0.57}$, i.e. a bit faster than the square root of the dynamic pressure, so that it may

575 reasonably be supposed that a sharp increase in the plasma sheet current density produced by
576 a dynamic pressure increase could trigger an instability starting or simply increasing the
577 reconnection rate. The velocity of the plasma flowing out of the reconnection site is, in a first
578 approximation, the Alfvén speed $V_A = B/(\mu_0 \rho)^{1/2}$, and under the frozen-in approximation, the
579 electric field is, $E_y \sim B_z V_A$ [Owen and Cowley, 1987]. The effect of compression is to
580 increase both the magnetic field and the plasma density. If in addition we assume that the
581 field and the density increase at roughly the same rate (i.e. a doubling of the field would take
582 place along with a doubling of the plasma density), then we can expect that V_A will also be
583 increased by the compression (for example, a doubling of both B and ρ increases V_A by a
584 factor ~ 1.41). We do not expect that B_z would be much increased by the compression
585 because, in a slightly idealized view of the magnetotail, the magnetic effect of compression is
586 to move field lines roughly parallel to the plasma sheet closer to each other, modifying the
587 magnetic flux threading a surface element perpendicular to the sheet. It follows that the newly
588 closed field lines are efficiently evacuated from the reconnection site due to higher V_A . It also
589 follows that a larger electric field can be expected in the vicinity of the reconnection site when
590 the plasma sheet is compressed, consistently with the increase of the Alfvén speed that results
591 from the competing increase of both the plasma density and magnetic field, suggesting an
592 increased reconnection rate. In addition, one could also speculate that a stronger compression
593 of the tail could lead to the formation of a reconnection site of larger extent favouring a larger
594 value of the extreme rate of flux closure.

595 6. Discussion

596 A statistical study, and especially a statistical correlation study, must be analyzed
597 considering the possible physical mechanisms that lead to a correlation between two
598 parameters. Two quantities can be found to be correlated despite the lack of causal relation
599 between them. Moreover, for large data samples, statistical tests very often indicate the
600 presence of a correlation between variables that are obviously unrelated on physical grounds.
601 In the present study, a very large number of parameters were defined and correlated with each
602 other. We restricted our manuscript to the most significant and physically meaningful
603 correlations. Proceeding this way, we may have excluded correlations between parameters
604 that are truly related on physical grounds but for which the scatter of the dataset does not
605 allow us to identify a strong correlation. On the other hand, the most significant correlations
606 that we presented very likely rely on physical processes.

607 In our search for a criterion allowing discriminating between strong and weak solar
608 wind dynamic pressure pulses, several criteria were proposed. This could appear to be an
609 inconsistency, because one would expect to find a single criterion. However, the concept of a
610 strong dynamic pressure pulse is somewhat imprecise, and the complexity of the coupled
611 solar wind – magnetosphere system is such that the response of the magnetosphere cannot be
612 fully determined by a single parameter. It is thus not unacceptable to consider that strong
613 pressure pulses can be defined according to several criteria that will not necessarily be
614 simultaneously fulfilled. Indeed, as we already mentioned above, our identification of
615 dynamic pressure pulses based on the excitation of a dayside subauroral proton flash also
616 selects intervals with a rather weak dynamic pressure variation that does not much compress
617 the tail and can be considered simply as a trigger that switches on the process of relaxation of
618 the loaded magnetosphere. For these cases, it is not surprising to find that the flux closure
619 process mostly correlates with parameters representing the initial state of the magnetosphere,
620 i.e. its preconditioning. For stronger dynamic pressure pulses, the preconditioning of the
621 magnetosphere still plays a role, but the properties of the dynamic pressure front are of
622 importance as well.

623 Initially the most natural criterion for identification of strong dynamic pressure pulses
624 is certainly that based on the dynamic pressure increase. However, the time scale in which the
625 dynamic pressure increase takes place is also important. In this study, this aspect did not have
626 to be explicitly considered because solar wind dynamic pressure pulses were identified based
627 on a pragmatic observational criterion: we searched for dayside subauroral proton flashes to
628 identify pulses. Consequently, the time scale limitation was implicitly included in the process
629 of events selection: every selected interval did include a dynamic pressure variation that
630 caused a rapid compression of the dayside magnetosphere, and could thus be considered as a
631 dynamic pressure front, i.e. presenting a rapid variation of the pressure exerted by the solar
632 wind on the magnetosphere. The dynamic pressure variation that we determined for our set of
633 intervals thus always did take place on a sufficiently short time scale for the purpose of this
634 study. A typical time scale can nevertheless be roughly estimated using the criterion based on
635 the maximum rate of change of the solar wind dynamic pressure. We found strong pulse
636 criteria to be $\Delta P_{dyn} > 2.8 \text{ nPa}$, and $\left. \frac{dP_{dyn}}{dt} \right|_{\max} > 2.14 \times 10^{-2} \text{ nPa/s}$. The ratio of these two
637 thresholds is 131 s. The typical time scale on which the dynamic pressure increase must take
638 place is thus of the order of a few minutes.

639 The results obtained here on statistical grounds are in good agreement with previous
640 studies. Clearly we find that flux closure takes place in response to the interaction between the
641 magnetosphere and solar wind dynamic pressure fronts, as in previous studies by *Boudouridis*
642 *et al.* [2003, 2004]. Although the auroral precipitation and flux closure are two different
643 signatures of that interaction, we find, along the same lines as *Meurant et al.* [2004], that
644 weak pressure pulses play only a triggering role on magnetic flux closure, in such a manner
645 that the detailed properties of the solar wind pressure front have a minor influence on the
646 magnetospheric response, compared with the influence of the initial state of the
647 magnetosphere. However, we find that, in the case of a strong pressure pulse, the pulse does
648 not only trigger the reconnection process in the tail, but also the solar wind properties
649 significantly influence the magnetospheric response expressed in terms of flux closure, in
650 contrast with *Meurant et al.* [2004]. We also find that a change of the IMF magnitude is an
651 important parameter for dynamic pressure pulse-induced flux closure, especially for the
652 intensification of the flux closure rate. For strong pulses, the solar wind velocity, and
653 especially its variation, significantly influences the process of dynamic pressure pulse-
654 induced flux closure, which recalls the results obtained by *Meurant et al.* [2004] concerning
655 the auroral precipitation. On the effect of the preconditioning, we find that the amount of open
656 flux available for closure prior to the arrival of a solar wind pressure front is a key parameter
657 in the case of a weak pulse, along the same line as the results previously found by *Meurant et*
658 *al.* [2004] for the B_z IMF component. In addition, we find that the size of the magnetospheric
659 cavity also plays a preconditioning role in the case of a weak pressure pulse.

660 7. Conclusions

661 We conducted a statistical study of the flux closure in the tail related to solar wind
662 dynamic pressure fronts. We found that the response of the magnetotail (in terms of flux
663 closure) to a solar wind dynamic pressure front is mainly governed by the preconditioning of
664 the magnetosphere in the case of weak pressure pulses ($\Delta P_{dyn} < 2.8$ nPa) whereas the
665 properties of the solar wind become key parameters in the case of strong pulses ($\Delta P_{dyn} > 2.8$
666 nPa, taking place at the time scale of a few minutes). Indeed, strong pulses are capable of
667 significantly compressing the geomagnetic tail, which vigorously stimulates magnetic
668 reconnection in the plasma sheet. Geosynchronous data also show that the compression of the
669 tail stimulates flux closure. In the case of a weak pulse, the preconditioning of the
670 magnetosphere relies both on the amount of open flux accumulated prior to the arrival of the
671 dynamic pressure front, and on the size of the magnetospheric cavity. In the case of a strong

672 dynamic pressure pulse, the solar wind velocity, and especially its variation, is the solar wind
673 property that influences the process of flux closure the most, although the variation of the
674 solar wind dynamic pressure is also an important factor. The availability of open flux remains
675 however a limiting factor. We also find that an intensification of the IMF favours the process
676 of flux closure, but this may not be a specific feature of dynamic pressure pulse-induced flux
677 closure intervals.

678

679 *Acknowledgements* The success of the IMAGE mission is a tribute to the many dedicated
680 scientists and engineers that have worked and continue to work on the project. The PI for the
681 mission is Dr J.L. Burch. Jean-Claude Gérard and Benoît Hubert are supported by the Belgian
682 National Fund for Scientific Research (FNRS). This work was funded by the PRODEX
683 program of the European Space Agency (ESA). Work at Leicester was supported by STFC
684 grant PP/E000983/1. ACE level 2 data were provided by N.F. Ness (MFI) and D.J. McComas
685 (SWEPAM), and the ACE Science Centre. GOES-8 data were obtained thanks to CDAWeb.

686 References

- 687 Blockx C., J.-C. Gérard, V. Coumans, B. Hubert, M. Meurant (2009), Contributions of the
688 driven process and the loading-unloading process during substorms: A study based on the
689 IMAGE-SI12 imager, *J. Geophys. Res.*, 114, A02209, doi:10.1029/2008JA013280.
- 690 Boudouridis, A., E. Zesta, L. Lyons, P. Anderson, and D. Lummerzheim (2003), Effect of
691 solar wind pressure pulses on the size and strength of the auroral oval, *J. Geophys. Res.*,
692 108(A4), CiteID 8012, doi:10.1029/2002JA009373.
- 693 Boudouridis, A., E. Zesta, L. R. Lyons, P. C. Anderson, and D. Lummerzheim (2004),
694 Magnetospheric reconnection driven by solar wind pressure fronts, *Ann. Geophys.*, 22,
695 1367-1378.
- 696 Brittnacher, M., M. Wilber, M. Fillingim, D. Chua, G. Parks, J. Spann, and G. Germany
697 (2000), Global auroral response to a solar wind pressure pulse, *Adv. Space Res.*, 25, 1377-
698 1385.
- 699 Cowley, S.W.H. and M. Lockwood, Excitation and decay of solar wind-driven flows in the
700 magnetosphere-ionosphere system (1992), *Ann. Geophys.*, 10, 103-115.
- 701 Feldman W. C., J. R. Asbridge, S. J. Bame, and J. T. Gosling (1977), Plasma and magnetic
702 fields from the sun, in *The Solar Output and its Variation*, edited by O. R. White, pp. 351-
703 382, Colorado Associated University Press, Boulder.
- 704 Fuselier, S. A., S. P. Gary, M. F. Thomsen, E. S. Claflin, B. Hubert, B. R. Sandel, and T.
705 Immel (2004), Generation of Transient Dayside Sub-Auroral Proton Precipitation, *J.*
706 *Geophys. Res.*, 109, A1227, doi:10.1029/2004JA010393.
- 707 Hubert, B., J.-C. Gérard, S. A. Fuselier, S. B. Mende (2003), Observation of dayside
708 subauroral proton flashes with the IMAGE-FUV imagers, *Geophys. Res. Lett.*, 30, doi:
709 10.1029/2002GL016464.
- 710 Hubert, B., S. E. Milan, A. Grocott, C. Blockx, S. W. H. Cowley, and J.-C. Gérard (2006a),
711 Dayside and nightside reconnection rates inferred from IMAGE FUV and Super Dual
712 Auroral Radar Network data, *J. Geophys. Res.*, 111, A03217,
713 doi:10.1029/2005JA011140.
- 714 Hubert B., M. Palmroth, T.V. Laitinen, P. Janhunen, S.E. Milan, A. Grocott, S.W.H. Cowley,
715 T. Pulkkinen, and J.-C. Gérard (2006b), Compression of the Earth's magnetotail by
716 interplanetary shocks directly drives transient magnetic flux closure, *Geophys. Res. Lett.*,
717 33, L10105, doi:10.1029/2006GL026008.
- 718 Kivelson, M. G. and C. T. Russell, *Introduction to space physics*, Cambridge University
719 Press, Cambridge, UK, 1997.
- 720 Meurant, M.; J. C. Gérard; B. Hubert; V. Coumans; V. I. Shematovich; D. V. Bisikalo, D. S.
721 Evans, G. R. Gladstone, S. B. Mende (2003), Characterization and dynamics of the
722 auroral electron precipitation during substorms deduced from IMAGE-FUV, *J. Geophys.*
723 *Res.*, 108, 1247, doi: 10.1029/2002JA009685.

- 724 Meurant, M.;J.-C. Gérard, B. Hubert, V. Coumans, C. Blockx, N. Østgaard, S. B. Mende
725 (2003), Dynamics of global scale electron and proton precipitation induced by a solar
726 wind pressure pulse, *Geophys. Res. Lett.*, 30, 2032 10.1029/2003GL018017.
- 727 Meurant, M., J.-C. Gérard, C. Blockx, B. Hubert, and V. Coumans (2004), Propagation of
728 electron and proton shock-induced aurora and the role of the interplanetary magnetic field
729 and solar wind, *J. Geophys. Res.*, 109, A10210, doi:10.1029/2004JA010453.
- 730 Mende, S.B., H. Heeterks, H.U. Frey, M. Lampton, S.P. Geller, S. Habraken, E. Renotte, C.
731 Jamar, P. Rochus, J. Spann, S.A. Fuselier, J.C. Gérard, G.R. Gladstone, S. Murphree, and
732 L. Cogger (2000a), Far ultraviolet imaging from the IMAGE spacecraft: 1. System
733 design, *Space Sci. Rev.*, 91, 243-270.
- 734 Mende, S.B., H. Heeterks, H.U. Frey, J.M. Stock, M. Lampton, S. Geller, R. Abiad, O.
735 Siegmund, S. Habraken, E. Renotte, C. Jamar, P. Rochus, J.C. Gérard, R. Sigler, and H.
736 Lauche (2000b), Far ultraviolet imaging from the IMAGE spacecraft : 3. Spectral
737 imaging of Lyman alpha and OI 135.6 nm, *Space Sci. Rev.*, 91, 287-318.
- 738 Owen, C. J., and S. W. H. Cowley (1987), Simple models of time-dependent reconnection in
739 a collision-free plasma with an application to substorms in the geomagnetic tail, *Planet.*
740 *Space Sci.*, 35, 451-466.
- 741 Petrinec, S. M., and C. T. Russell (1993), An empirical model of the size and shape of the
742 near-Earth magnetotail, *Geophys. Res. Lett.*, 20, 2695-2698.
- 743 Petrinec, S. M., and C. T. Russell (1996), Near-Earth magnetotail shape and size as
744 determined from the magnetopause flaring angle, *J. Geophys. Res.*, 101, 137-152.
- 745 Ruohoniemi, J. M., and K.B. Baker (1998), Large scale imaging of high latitude convection
746 with Super Dual Auroral Radar Network HF radar observations, *J. Geophys. Res.*, 103,
747 20797-20811.
- 748 Savitzky A. and M.J.E. Golay (1964), Smoothing and differentiation of data by simplified
749 least squares procedures, *Anal. Chem.*, 36,1627-1639, doi: 10.1021/ac60214a047.
- 750

Symbol	Definition
n_{sw}	Solar wind numeric density
v_{sw}	Solar wind bulk velocity
$v_{sw, init}$	Initial value of v_{sw} , i.e. prior the the dynamic pressure pulse arrival
$v_{sw, max}$	Maximum value reached by v_{sw} after the dynamic pressure pulse arrival
Δv_{sw}	Variation of v_{sw} associated with the pressure pulse: $\Delta v_{sw} = v_{sw, max} - v_{sw, init}$
$\Delta v_{sw} \Big _{ramp}$	Variation of v_{sw} over the ramp of the solar wind dynamic pressure pulse
P_{dyn}	Solar wind dynamic pressure
ΔP_{dyn}	Variation of P_{dyn} (pressure jump)
$P_{dyn, max}$	Maximum value of P_{dyn} over a given time interval
$\frac{dP_{dyn}}{dt} \Big _{max}$	Maximum value of the time derivative of P_{dyn} over a given time interval
$B_z, max(min)$	Maximum (minimum, respectively) value of B_z over a given time interval
$\Delta B $	Variation of the IMF intensity over a given time interval
$\frac{d B }{dt} \Big _{ramp}$	Averga rate of change of the IMF intensity during the ramp of the solar wind dynamic pressure pulse
R_M	Radius of the magnetopause, i.e. standoff distance of the magnetopause
$R_{M, max}$	Maximum value of R_M over a given time interval
R_B	Radius of the bow shock, i.e. standoff distance of the bow shock
Φ	Open magnetic flux
Φ_{init}	Initial value of Φ prior to the solar wind dynamic pressure pulse arrival
Φ_{final}	Final value of Φ at the end of the pulse-induced flux closure interval
$\Delta\Phi$	$\Phi_{final} - \Phi_{init}$
V_{cl}	Magnetic flux closure voltage (a negative number)
$\overline{V_{cl}}$ and $\underline{V_{cl}}$	Average and median values (resp.) of V_{cl} over a given time interval.
$V_{cl, min}$	Minimum value of V_{cl} during a given time interval
$V_{cl, init}$	V_{cl} initial value, i.e. prior to the solar wind dynamic pressure pulse arrival
ΔV_{cl}	$V_{cl, min} - V_{cl, init}$: intensification of V_{cl} during the dynamic pressure pulse-induced flux closure interval.
Φ_{cl}	Amount of open flux closed during a given time interval. $\Phi_{cl} = \int_{t_0}^{t_1} V_{cl} dt$
V_{op}	Magnetic flux opening voltage
Φ_{op}	Amount of open flux created during a given time interval. $\Phi_{op} = \int_{t_0}^{t_1} V_{op} dt$
e	Elevation angle of the geomagnetic field at geosynchronous altitude from the GOES-8 measurements
e_{init}	Initial value of e , i.e. prior to the dynamic pressure pulse arrival
e_{min}	Minimum value of e over a given time interval
$\frac{de}{dt} \Big _{min}$	Minimum value of the time derivative of e over a given time interval
Δe_{ramp}	Variation of e during the ramp of the solar wind dynamic pressure pulse

752 Table 1. List of symbols used in this study.

753

Φ_{final}	r	α
Φ_{init}	0.807	>0.999
B_z_{max}	-0.414	0.999
ΔP_{dyn}	-0.307	0.991
$P_{dyn,max}$	-0.298	0.988

754 Table 2. Correlation coefficients (r) and levels of confidence (α) for Φ_{final} with Φ_{init} , B_z_{max} ,
 755 ΔP_{dyn} , and $P_{dyn,max}$. α is the worst of the Fisher and the Student tests.

756

	Φ_{cl}		$\Delta\Phi$	
	r	α	r	α
Φ_{init}	-0.397	0.999	-0.410	0.999
$R_{M,max}$	-0.324	0.988	-0.332	0.990
Φ_{op}	-0.214	0.913	-0.06	0.612

757 Table 3. Correlation coefficients (r) and levels of confidence (α) for Φ_{cl} and $\Delta\Phi$ with Φ_{init} ,
 758 $R_{M,max}$, and Φ_{op} . α is the worst of the Fisher and the Student tests.

759

	$\overline{V_{cl}}$		$\underline{V_{cl}}$	
	r	α	r	α
Φ_{init}	-0.456	> 0.999	-0.417	0.999
$R_{M,max}$	-0.410	0.999	-0.407	0.999
$R_{B,max}$	-0.408	0.999	-0.406	0.999

760 Table 4. Correlation coefficients (r) and levels of confidence (α) for $\overline{V_{cl}}$ and $\Delta\Phi$ with Φ_{init} ,
 761 $R_{M,max}$, and $R_{B,max}$. α is the worst of the Fisher and the Student tests.

762

$V_{cl,min}$	r	α
Φ_{init}	-0.334	0.993
$R_{M,max}$	-0.415	0.999
$R_{B,max}$	-0.412	0.999
$\Delta/B $	-0.335	0.993
$\frac{d B }{dt}\Big _{ramp}$	-0.344	0.995
$\Delta v_{sw}\Big _{ramp}$	-0.321	0.991

763 Table 5. Correlation coefficients (r) and levels of confidence (α) for $V_{cl,min}$ with Φ_{init} , $R_{M,max}$,
 764 $R_{B,max}$, $\Delta/B|$, $\frac{d|B|}{dt}\Big|_{ramp}$, and $\Delta v_{sw}\Big|_{ramp}$. α is the worst of the Fisher and the Student tests.

765

ΔV_{cl}	r	α
$\Delta/B/$	-0.352	0.996
$\Delta v_{sw} _{ramp}$	-0.300	0.985
Φ_{op}	-0.356	0.996

766 Table 6. Correlation coefficients (r) and levels of confidence (α) for ΔV_{cl} with $\Delta/B/$,
767 $\Delta v_{sw}|_{ramp}$, and Φ_{op} . α is the worst of the Fisher and the Student tests.

768

ΔP_{dyn}		r	α
Full dataset	ΔV_{cl}	-0.166	0.827
	Φ_{cl}	-0.138	0.741
$\Delta P_{dyn} > \sim 2.8$ nPa	ΔV_{cl}	-0.495	0.998
	Φ_{cl}	-0.490	0.987

769 Table 7. Correlation coefficients (r) and levels of confidence (α) for ΔP_{dyn} with ΔV_{cl} and Φ_{cl}
770 for the full dataset (upper lines) and for the subset of data for which $\Delta P_{dyn} > \sim 2.8$ nPa (lower
771 lines). α is the worst of the Fisher and the Student tests.

772

ΔP_{dyn}	Threshold (nPa)	r	α
ΔV_{cl}	2.8	-0.495	0.9982
$V_{cl,min}$	2.8	-0.278	0.9045
Φ_{cl}	2.8	-0.340	0.9575
$\overline{V_{cl}}$	3	-0.220	0.7898
$\underline{V_{cl}}$	3	-0.283	0.8958
$\Delta\Phi$	2.8	-0.162	0.6752

773 Table 8. Subset thresholds and correlations for ΔP_{dyn} . The correlation coefficient r and level
774 of confidence α of the Student test are obtained between ΔP_{dyn} and the quantities listed in
775 column 1 restricting the dataset to events for which ΔP_{dyn} is larger than the value listed in the
776 column labelled “Threshold”. These thresholds isolate the subset of events presenting the
777 highest correlation level of confidence for each pair of variables.

$\left. \frac{dP_{dyn}}{dt} \right _{max}$	Threshold (nPa/s)	r	α
ΔV_{cl}	2.14×10^{-2}	-0.584	0.9978
$V_{cl,min}$	2.14×10^{-2}	-0.465	0.9809
Φ_{cl}	2.14×10^{-2}	-0.490	0.9870
\overline{V}_{cl}	2.14×10^{-2}	-0.369	0.9304
\underline{V}_{cl}	1.80×10^{-2}	-0.344	0.9327
$\Delta \Phi$	1.80×10^{-2}	-0.251	0.8112

779 Table 9. Subset thresholds and correlations for $\left. \frac{dP_{dyn}}{dt} \right|_{max}$. The correlation coefficient r and
780 level of confidence α of the Student test are obtained between $\left. \frac{dP_{dyn}}{dt} \right|_{max}$ and the quantities
781 listed in column 1 restricting the dataset to events for which $\left. \frac{dP_{dyn}}{dt} \right|_{max}$ is larger than the value
782 listed in the column labelled “Threshold”. These thresholds isolate the subset of events
783 presenting the highest correlation level of confidence for each pair of variables.

784

P_{max}	Threshold (nPa)	r	α
ΔV_{cl}	5.97	-0.526	0.9972
$V_{cl,min}$	6.14	-0.345	0.9159
Φ_{cl}	5.97	-0.334	0.9283
\overline{V}_{cl}	6.14	-0.256	0.7932
\underline{V}_{cl}	6.14	-0.266	0.8109

785 Table 10. Subset thresholds and correlations for P_{max} . The correlation coefficient r and level
786 of confidence α of the Student test are obtained between P_{max} and the quantities listed in
787 column 1 restricting the dataset to events for which P_{max} is larger than the value listed in the
788 column labelled “Threshold”. These thresholds isolate the subset of events presenting the
789 highest correlation level of confidence for each pair of variables.

790

With $\Delta v_{sw} _{ramp}$	Threshold (km/s)	r	α
ΔV_{cl}	11.3	-0.586	0.9997
$V_{cl,min}$	11.3	-0.673	> 0.9999
Φ_{cl}	11.3	-0.638	0.9999
\overline{V}_{cl}	11.6	-0.692	>0.9999
\underline{V}_{cl}	12.0	-0.729	>0.9999

791 Table 11. Subset thresholds and correlations for $\Delta v_{sw}|_{ramp}$. The correlation coefficient r and
 792 level of confidence α of the Student test are obtained between $\Delta v_{sw}|_{ramp}$ and the quantities
 793 listed in column 1 restricting the dataset to events for which $\Delta v_{sw}|_{ramp}$ is larger than the value
 794 listed in the column labelled “Threshold”. These thresholds isolate the subset of events
 795 presenting the highest correlation level of confidence for each pair of variables.

796

With Δv_{sw}	Threshold (km/s)	r	α
ΔV_{cl}	8.6	-0.541	0.9983
$V_{cl,min}$	8.6	-0.577	0.9993
Φ_{cl}	8.6	-0.614	0.9998
\overline{V}_{cl}	8.6	-0.603	0.9997
\underline{V}_{cl}	8.6	-0.643	0.9999

797 Table 12. Subset thresholds and correlations for Δv_{sw} . The correlation coefficient r and level
 798 of confidence α of the Student test are obtained between Δv_{sw} and the quantities listed in
 799 column 1, restricting the dataset to events for which Δv_{sw} is larger than the value listed in the
 800 column labelled “Threshold”. The same threshold value was found to isolate the subset of
 801 events presenting the highest correlation level of confidence for each pair of variables.

802

With $\max\left(\frac{dv_{sw}}{dt}\right)$	Threshold (km/s ²)	r	α
ΔV_{cl}	0.222	-0.471	0.9900
$V_{cl,min}$	0.286	-0.686	0.9994
Φ_{cl}	0.286	-0.782	>0.9999
\overline{V}_{cl}	0.286	-0.738	0.9999
\underline{V}_{cl}	0.286	-0.695	0.9997

803 Table 13. Subset thresholds and correlations for $\max\left(\frac{dv_{sw}}{dt}\right)$. The correlation coefficient r
 804 and level of confidence α of the Student test are obtained between $\max\left(\frac{dv_{sw}}{dt}\right)$ and the
 805 quantities listed in column 1, restricting the dataset to events for which $\max\left(\frac{dv_{sw}}{dt}\right)$ is larger
 806 than the value listed in the column labelled “Threshold”.

807

$\Delta/B/$	Threshold (nT)	r	α
ΔV_{cl}	0.47	-0.724	> 0.9999
$V_{cl,min}$	0.47	-0.691	> 0.9999
Φ_{cl}	0.47	-0.676	0.9999
\overline{V}_{cl}	0.47	-0.678	0.9999
\underline{V}_{cl}	0.47	-0.724	> 0.9999

808 Table 14. Subset thresholds and correlations for $\Delta/B/$. The correlation coefficient r and level
 809 of confidence α of the Student test are obtained between $\Delta/B/$ and the quantities listed in
 810 column 1 restricting the dataset to events for which $\Delta/B/$ is larger than the value listed in the
 811 column labelled “Threshold”. These thresholds isolate the subset of events presenting the
 812 highest correlation level of confidence for each pair of variables.

813

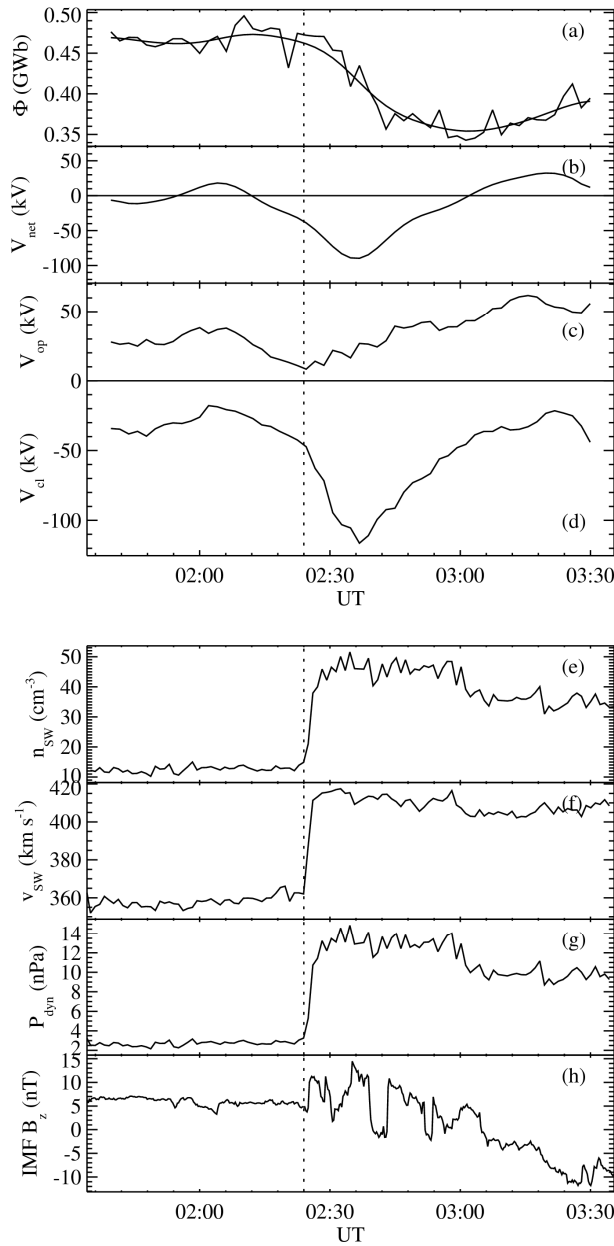
814

With Δv_{SW}	r	α
ΔV_{cl}	-0.554	> 0.999
$V_{cl,min}$	-0.613	> 0.999
Φ_{cl}	-0.621	> 0.999
\overline{V}_{cl}	-0.638	> 0.999
\underline{V}_{cl}	-0.678	> 0.999

815 Table 15. Correlation coefficients relating Δv_{SW} and several parameters describing the
 816 dynamic pressure pulse-induced flux closure, restricting the analysis to the subset for which
 817 $\Delta P_{dyn} > 2.8$ nPa. The reported level of confidence was computed applying the Student test. A
 818 correlation coefficient of ~ 0.999 is found applying the Fisher test.

819

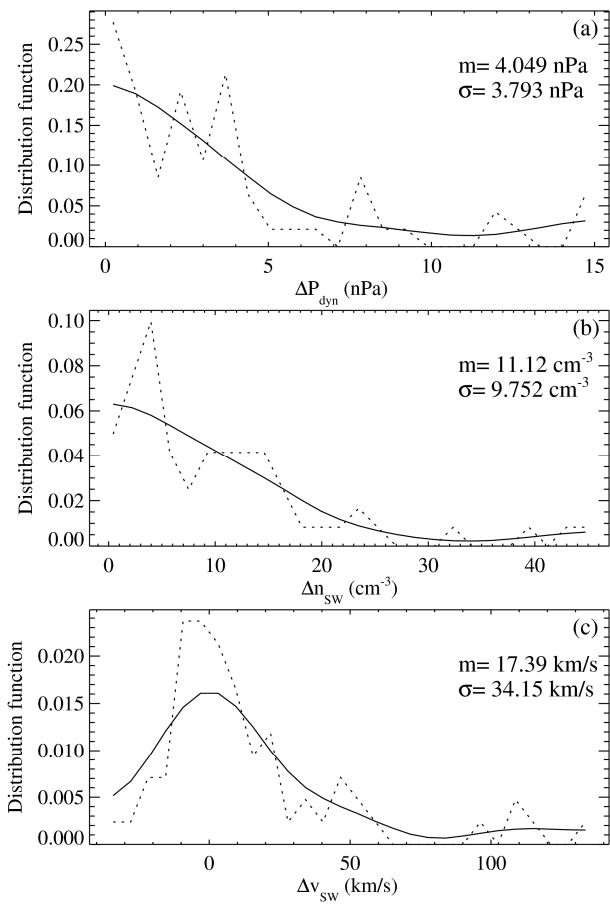
820 Figures and captions



821
 822 Figure 1. Dynamic pressure front recorded on 4
 823 November 2000: The upper panel shows (a) the
 824 open magnetic flux deduced from ionospheric and
 825 auroral observations, (b) the net reconnection
 826 voltage, (c) the flux opening rate, (d) the flux
 827 closure rate. The lower panel shows solar wind
 828 data from observations of the ACE satellite (e)
 829 density, (f) velocity, (g) dynamic pressure, and (h)
 830 IMF B_z component. A suitable time shift is
 831 applied to account for propagation of the solar
 832 wind from the ACE location to the planet.

833

834

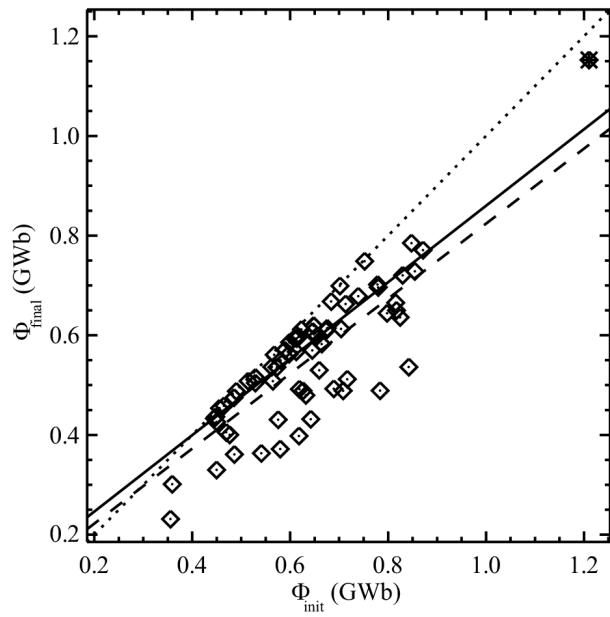


835

836 Figure 2. Statistical distribution function
837 (dotted lines) and smoothed statistical
838 distribution function (solid lines) of (a) the
839 solar wind dynamic pressure variation, (b) the
840 solar wind density variation, and (c) the solar
841 wind velocity variation for the selected set of
842 solar wind dynamic pressure pulses. The
843 average and standard deviation of the sample
844 is indicated for each variable.

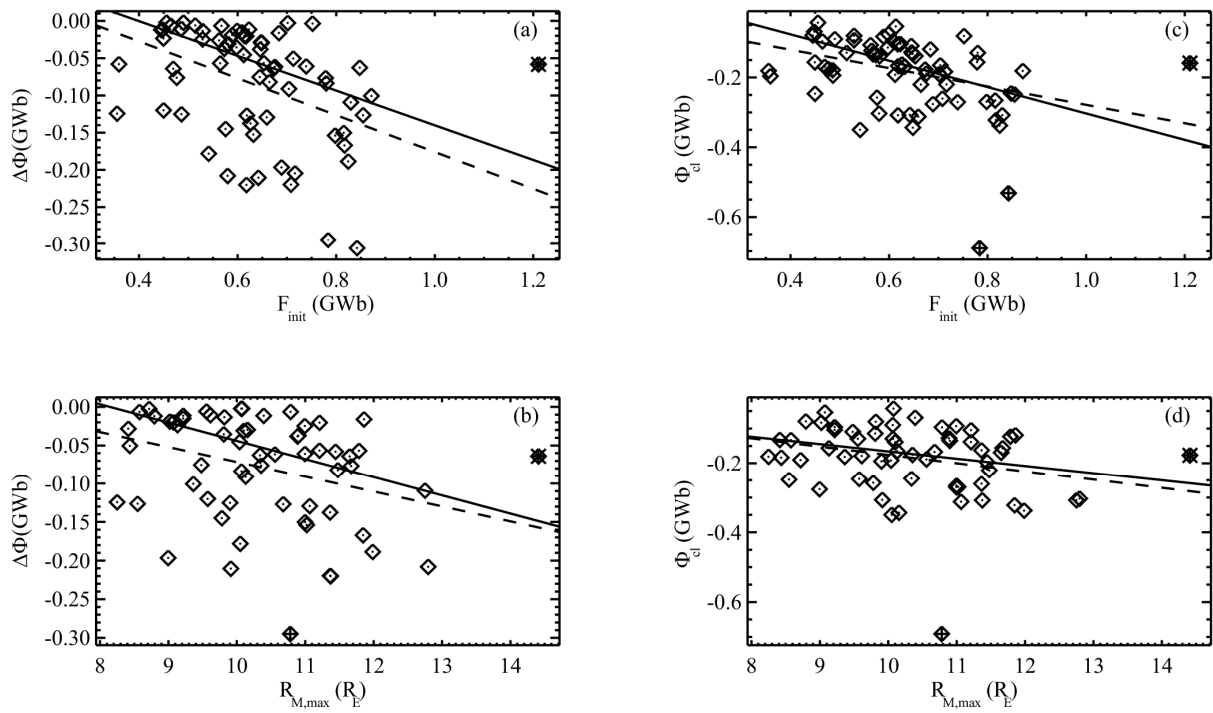
845

846



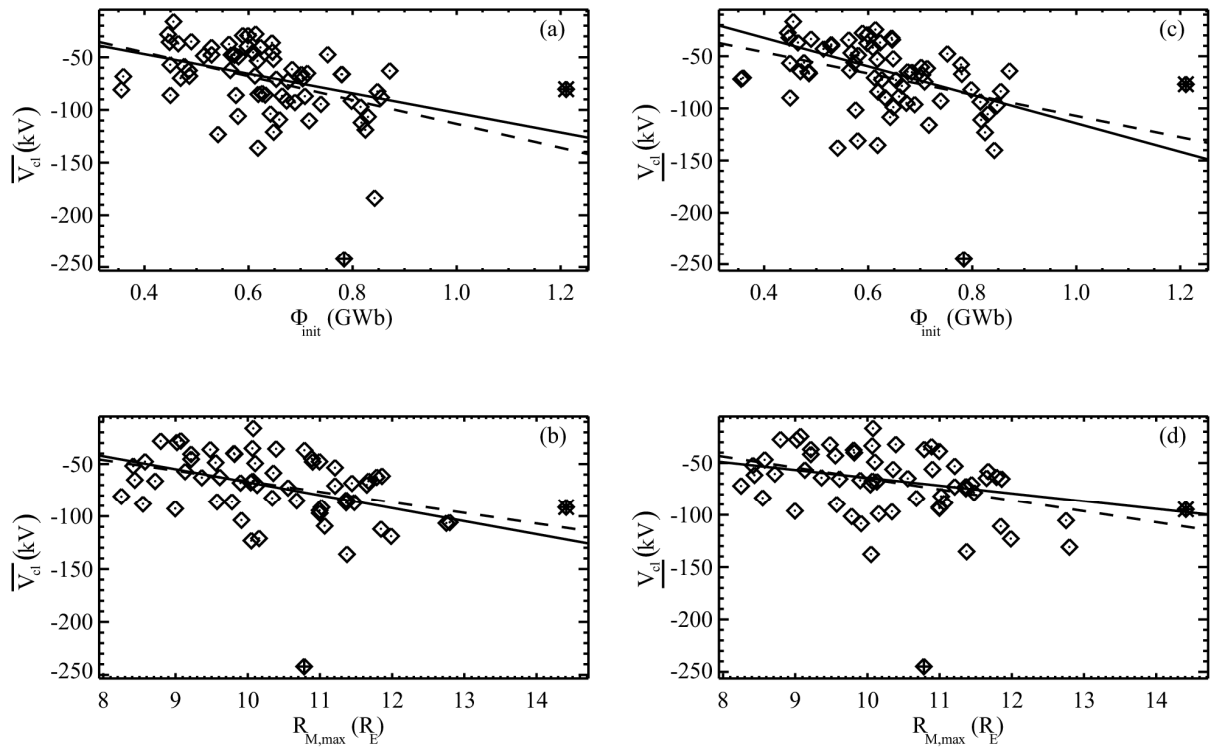
847

848 Figure 3. Final open flux as a function of the
 849 initial open flux. The data point overplotted with
 850 a * symbol is an outlier. The solid line indicates
 851 the least absolute deviation linear fit through the
 852 data points (excluding the outlier) and the
 853 dashed line is the regression line. The dotted
 854 line is the bisectrix.



856

857 Figure 4. Open flux variation ($\Delta\Phi$) as a function of the initial open flux Φ_{init} (a) and maximum
 858 magnetopause radius $R_{M,max}$ expressed in earth radii (b). Total amount of magnetic flux closed
 859 Φ_{cl} as a function of the initial open flux Φ_{init} (c) and maximum magnetopause radius $R_{M,max}$
 860 (d). Data points overplotted with a * or a + symbol are outliers. The solid lines are the least
 861 absolute deviation linear fits through the data points (excluding the outliers) and the dashed
 862 lines are the regression lines.

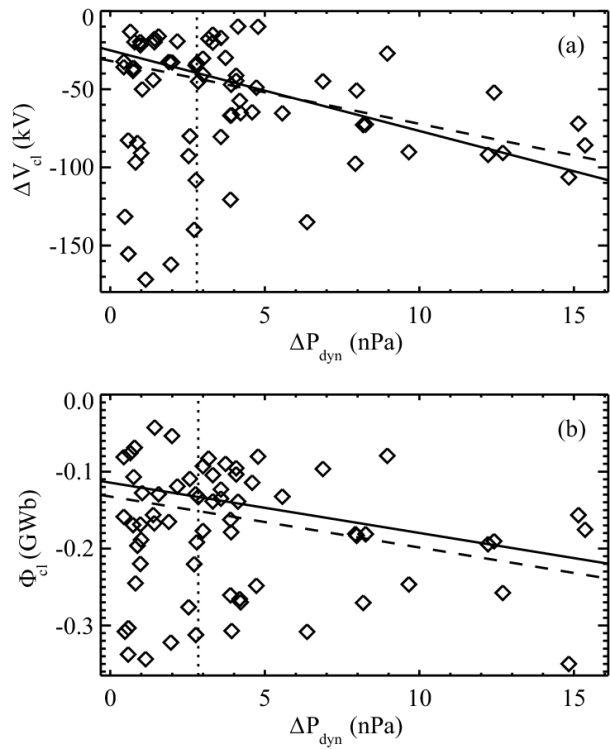


864

865 Figure 5. (a) Average closure voltage \overline{V}_{cl} as a function of the initial open flux Φ_{init} and (b) the
 866 maximum magnetopause radius $R_{M,max}$ expressed in earth radii, (c) median closure voltage \underline{V}_{cl}
 867 versus the initial open flux Φ_{init} and (d) maximum magnetopause radius $R_{M,max}$ (d). Data
 868 points overplotted with a * or a + symbol are outliers. The solid lines are the least absolute
 869 deviation linear fits through the data points (excluding the outliers) and the dashed lines are
 870 the regression lines.

871

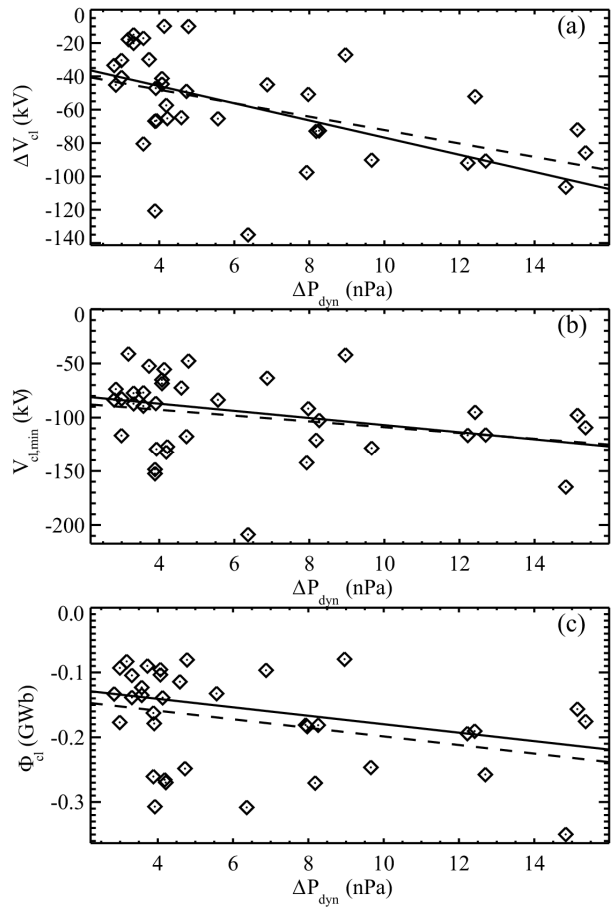
872



873

874 Figure 6. Closure voltage intensification (a) and amount of open flux closed (b) versus
 875 the solar wind dynamic pressure increase. The dotted vertical lines indicate a threshold of
 876 ~ 2.8 nPa, the solid and dashed lines are least absolute deviation fits and regression lines,
 877 respectively, through the data subset satisfying $\Delta P_{\text{dyn}} > 2.8$ nPa.

878



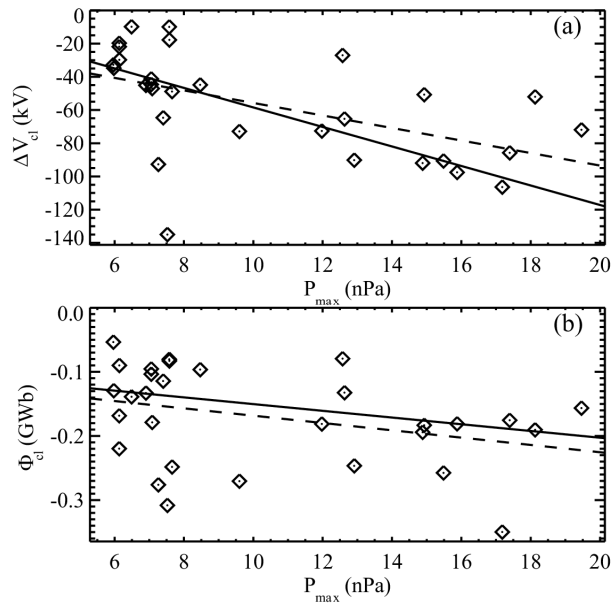
879

880 Figure 7. Closure voltage variation ΔV_{cl} (top panel), minimum closure voltage $V_{cl,min}$ (middle
 881 panel) and total amount of flux closed Φ_{cl} (bottom panel) as a function of the solar wind
 882 dynamic pressure increase ΔP_{dyn} , for the subset of events for which $\Delta P_{dyn} > 2.8$ nPa. Outliers
 883 were not plotted. The solid lines represent the least absolute deviation fits through the data.

884

885

886



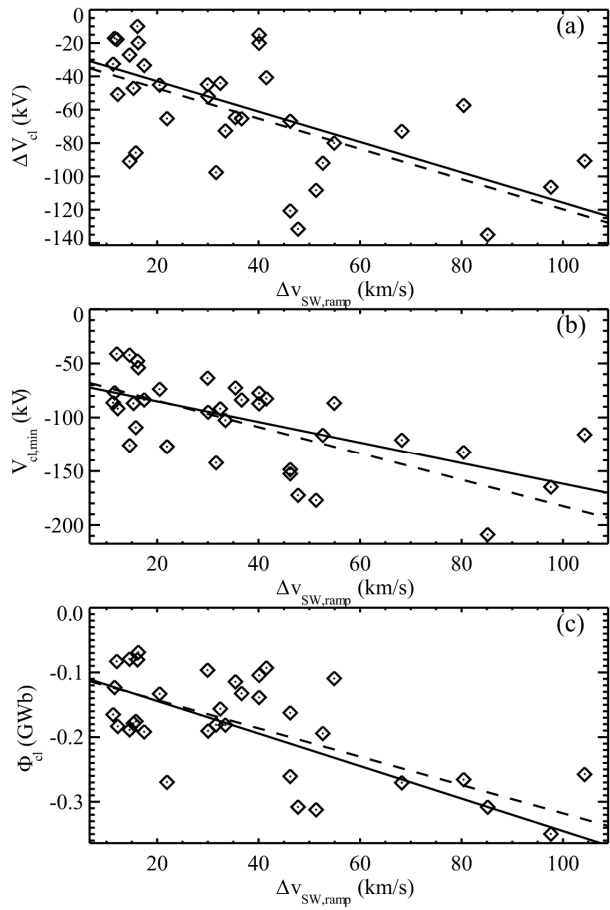
887

888 Figure 8. (a) Closure voltage variation ΔV_{cl} , and (b) total amount of flux closed Φ_{cl} as a
 889 function of the maximum solar wind dynamic pressure reached in each event $P_{dyn,max}$, for the
 890 subset of events for which $P_{dyn,max} > 5.97$ nPa. Outliers are not plotted. The solid lines
 891 represent the least absolute deviation fits through the data, and the dashed lines are the
 892 regression lines.

893

894

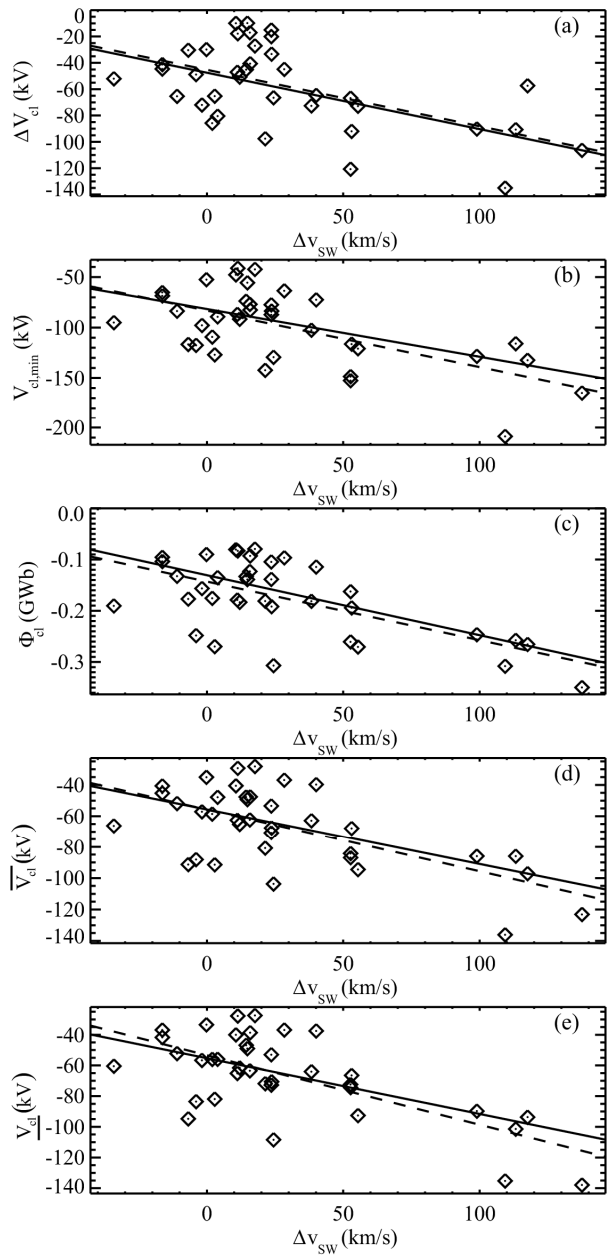
895



896

897 Figure 9. (a) Closure voltage variation ΔV_{cl} , (b) minimum closure voltage $V_{cl,min}$ and (c) total
 898 amount of flux closed Φ_{cl} as a function of the solar wind velocity variation during the ramp of
 899 the solar wind dynamic pressure pulse, for the subset of events for which $\Delta v_{SW,ramp} > 11.3$
 900 km/s. Outliers are not plotted. The solid lines represent the least absolute deviation fits
 901 through the data, and the dashed lines are the regression lines.

902



903

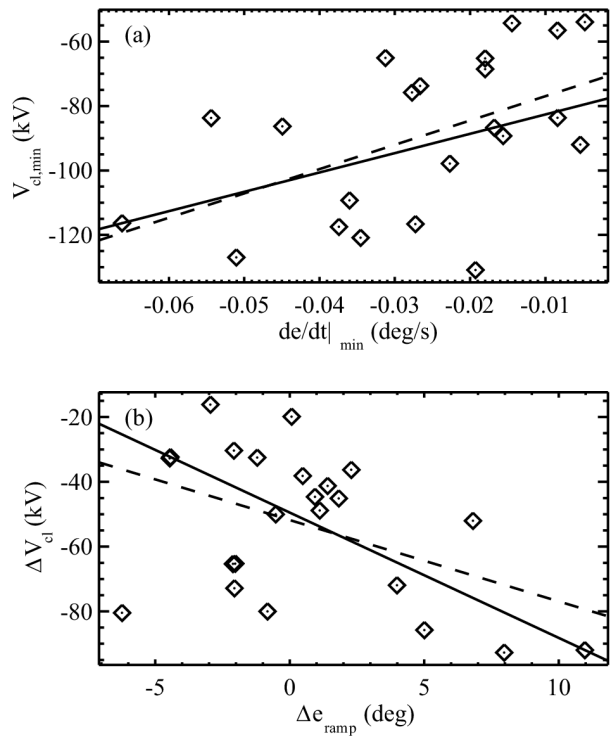
904 Figure 10. (a) Closure voltage variation ΔV_{cl} , (b) minimum closure voltage $V_{cl,min}$, (c) total
 905 amount of flux closed, (d) average closure voltage \overline{V}_{cl} , and (e) median closure voltage \underline{V}_{cl}
 906 versus the variation of the solar wind velocity Δv_{sw} , for the subset of events for which the
 907 variation of the solar wind dynamic pressure is $\Delta P_{dyn} > 2.8$ nPa. Outliers are not plotted. The
 908 solid lines represent the least absolute deviation fits through the data, and the dashed lines are
 909 the regression lines.

910

911

912

913



914

915 Figure 11. (a) Minimum closure voltage versus the minimum rate of change of the elevation
 916 angle deduced from GOES-8 measurements, and (b) the closure voltage intensification versus
 917 the variation of the elevation angle during the ramp of the solar wind dynamic pressure pulse,
 918 deduced from GOES-8 measurements. The solid lines are the least absolute deviation fits to
 919 the data, and the dashed lines are the regression lines. Outliers are not plotted.

920

921

922